

# Development and uncertainty quantification of hurricane surge response functions for hazard assessment in coastal bays

Nick R. Taylor · Jennifer L. Irish · Ikpoto E. Udoh ·  
Matthew V. Bilskie · Scott C. Hagen

Received: 28 May 2014 / Accepted: 3 February 2015 / Published online: 12 February 2015  
© Springer Science+Business Media Dordrecht 2015

**Abstract** Reliable and robust methods of extreme value-based hurricane surge prediction, such as the joint probability method (JPM), are critical in the coastal engineering profession. The JPM has become the preferred surge hazard assessment method in the USA; however, it has a high computational cost: One location can require hundreds of simulated storms and more than ten thousand computational hours to complete. Optimal sampling methods that use physics-based surge response functions (SRFs) can reduce the required number of simulations. This study extends the development of SRFs to bay interior locations at Panama City, Florida. Mean SRF root-mean-square errors for open coast and bay interior locations were 0.34 and 0.37 m, respectively, comparable with ADCIRC errors. Average uncertainty increases from open coast, and bay SRFs were 10 and 12 %, respectively. Long-term climate trends, such as rising sea levels, introduce nonstationarity into the simulated and historical surge datasets. A common approach to estimating total flood elevations is to take the sum of projected sea-level rise (SLR) and present day surge (static approach); however, this does not account for dynamic SLR effects on surge generation. This study demonstrates that SLR has a significant dynamic effect on surge in the Panama City area, and that total flood elevations, with respect to changes in SLR, are poorly characterized as static increases. A simple adjustment relating total flood elevation to present day conditions is proposed. Uncertainty contributions from these SLR adjustments are shown to be reasonable for surge hazard assessments.

**Keywords** Storm surge · Hazard assessment · Coastal flooding · Uncertainty · Hurricanes

---

N. R. Taylor · J. L. Irish (✉)  
Department of Civil and Environmental Engineering, Virginia Tech, Blacksburg, VA 24061, USA  
e-mail: jirish@vt.edu

I. E. Udoh  
Department of Civil Engineering, Texas A&M University, College Station, TX 77843, USA

M. V. Bilskie · S. C. Hagen  
Department of Civil, Environmental, and Construction Engineering, University of Central Florida,  
Orlando, FL, USA

**List of symbols**

EVA	Extreme value analysis
JPM	Joint probability method
OS	Optimal sampling
JPM-OS	Joint probability method with optimal sampling
SRF	Surge response function
SLR	Sea-level rise
MSL	Mean sea level
SST	Sea surface temperature
IPCC	Intergovernmental Panel on Climate Change
NOAA	National Oceanic and Atmospheric Administration
LCLU	Land cover-land use
PDF	Probability density function
RMS	Root-mean-square
$a_1, a_2$	Gumbel coefficients
$Z$	Total maximum flood elevation
$T_Z$	Total maximum flood elevation return period
$x$	Location of interest
$\phi$	SRF model term
$c_p$	Hurricane central pressure
$R_p$	Hurricane radius of maximum winds
$v_f$	Hurricane forward velocity
$\theta$	Hurricane track angle
$x_0$	Hurricane landfall position
$x'$	Dimensionless alongshore parameter
$\zeta'$	Dimensionless surge parameter
$\zeta$	Peak surge elevation
$\lambda(x_0)$	Ratio between relative maximum peak surge location and $R_p$
$c$	Dimensionless regional scaling constant
$L_{30}$	Cross-shore distance from shoreline to 30-m bathymetric contour, at $x_0$
$L_{30\text{-ref}}$	Threshold value of $L_{30}$
$R_{\text{thres}}$	Threshold value of $R_p$
$a_1, a_2, b_1, b_2$	Dimensionless scaling coefficients
$m_2, \alpha, \beta$	Dimensionless scaling coefficients
$\Delta p$	Ambient pressure and hurricane central pressure difference
$\Delta p_{\text{max}}$	Maximum theoretical hurricane intensity (Tonkin et al. 2000)
$[R_p/L_{30}]_{\text{ref}}$	Maximum value of $R_p/L_{30}$
$\gamma_0$	Reference specific weight of water
$\varepsilon_z$	Epistemic uncertainty
$\varepsilon_{\text{tide}}$	Tide model uncertainty
$\varepsilon_{\text{model}}$	Hydrodynamic and wind model uncertainty
$\varepsilon_{\text{waves}}$	Wave model uncertainty
$\varepsilon_{\text{wind}}$	Wind model uncertainty
$\varepsilon_{\text{residual}}$	Residual uncertainty
$\varepsilon_{\text{SRF}}$	SRF uncertainty
$\varepsilon_{\text{SLR}}$	SLR model uncertainty
$\mu$	Mean of normal distribution
$\sigma^2$	Variance of normal distribution

$Z_{SLR}$	Total flood elevation at projected SLR, relative to present day MSL
$Z_0$	Present day total flood elevation
$k, l$	Location-dependent fit coefficients

## 1 Introduction and background

Hurricanes continue to pose one of the most substantial risks to coastal communities, and the surges caused by these intense storms are a primary source of catastrophic damage. Reliable and robust methods of hurricane surge estimation are critical in reducing the damage that these storms inflict on lives and property. To obtain accurate and robust surge hazard assessments, it is essential that the full range of meteorological hurricane possibilities be considered. In the past, extreme value analysis (EVA) methods applied single distributions to recorded historical surge data (e.g., Yang et al. 1970; Fallah et al. 1976). After Hurricane Katrina, attempts to improve the accuracy of return period-based estimates led to the prevalent use of the joint probability method (JPM) in the USA (e.g., Liu et al. 2006; Niedoroda et al. 2010). The JPM, which reduces statistical uncertainty in surge data by supplementing historical storms with simulated synthetic storms, is computationally demanding; optimal sampling (OS) techniques are used in conjunction with the JPM to reduce the number of required simulations (JPM-OS). Currently, OS techniques can be categorized into three primary groups; interpolation schemes (Resio et al. 2007; Condon and Sheng 2012), quadrature schemes (Toro et al. 2010), and surge response function (SRF) schemes (e.g., Resio et al. 2009; Irish et al. 2009).

Throughout this study, the terms “surge,” “sea-level rise,” and “total flood elevation” will be referred to. Sea-level rise (hereafter SLR) refers to the increase in eustatic mean water elevation (mean sea level, hereafter MSL), before hurricane effects are considered. SLR levels of zero indicate “present day” conditions. Surge is used to measure the water elevation increase due to hurricane effects alone and is measured relative to MSL. Total flood elevation includes both surge and SLR.

SLR influences on total flood elevation, as well as surge generation, will be classified as either “static” or “dynamic.” Static changes in the total flood elevation refer to circumstances where the total flood elevation is well characterized by the summation of SLR and present day surge. In this context, “static” implies that the difference in relative surge levels is zero. Dynamic changes in the total flood elevation refer to circumstances where the total flood elevation is not well characterized by the summation of SLR and present day surge, and the relative difference in surge levels deviates significantly from zero. Because the static situation causes the difference in relative surge levels to be zero, further discussion regarding SLR effects on surge generation refers to dynamic effects, unless explicitly stated otherwise.

This study seeks to incorporate the effects of SLR into the SRF approach, while making the most efficient use of the information from the hydrodynamic surge models. While future coastal evolution induced by SLR may have a significant impact on future coastal flooding (e.g., Woodruff et al. 2013; Bilskie et al. 2014), these effects are not considered here. The SRFs, developed initially for open coast locations, will be applied to alongshore bay locations. An approach for integrating SLR into the SRFs will also be introduced, in order to improve the accuracy of total flood elevation predictions at future projected SLR conditions. It will be shown that the dynamic SLR contributions to total flood elevations can be characterized by a simple adjustment model, at locations along the open coast and

bay interior. Finally, epistemic uncertainty contributions from the SRF model, and the SLR adjustment, will be presented to demonstrate that these error contributions are small.

### 1.1 Site description

This study focuses on an 89-km span of coastline in Panama City, FL (Bay County, Fig. 1). The region has a permanent population of approximately 160,000, as well as a substantial annual tourist population. Most of the region’s bathymetry features a continental shelf with gradual alongshore variation; to the west, shore normal distances between the coastline and the 30-m bathymetric contour ( $L_{30}$ ) range between 14 and 40 km. The rate of continental shelf expansion increases west of Panama City, with  $L_{30}$  values increasing from 21 to 66 km. Recent studies of the influence of SLR on coastal evolution in the Panama City area (Passeri et al. 2015) indicate that this area is likely to experience accretion over the next half century.

Panama City’s bay is subdivided into four conjoined bodies: West Bay, North Bay, East Bay, and St. Andrew Bay. A chain of barrier islands forms the St. Andrew Sound, an enclosed body of water with a single inlet, as well as the eastern section of St. Andrew Bay. West Bay, North Bay, East Bay, and St. Andrew Sound are shallow bays, with mean depths of 2.55, 3.58, 3.19, and 1.73 m, respectively. The mean depth of St. Andrew Bay is 6.15 m.

### 1.2 Sea-level rise trends

While estimates of extreme value probabilities for present day conditions, including low-frequency to high-frequency events, are critically important for short-term planning, long-

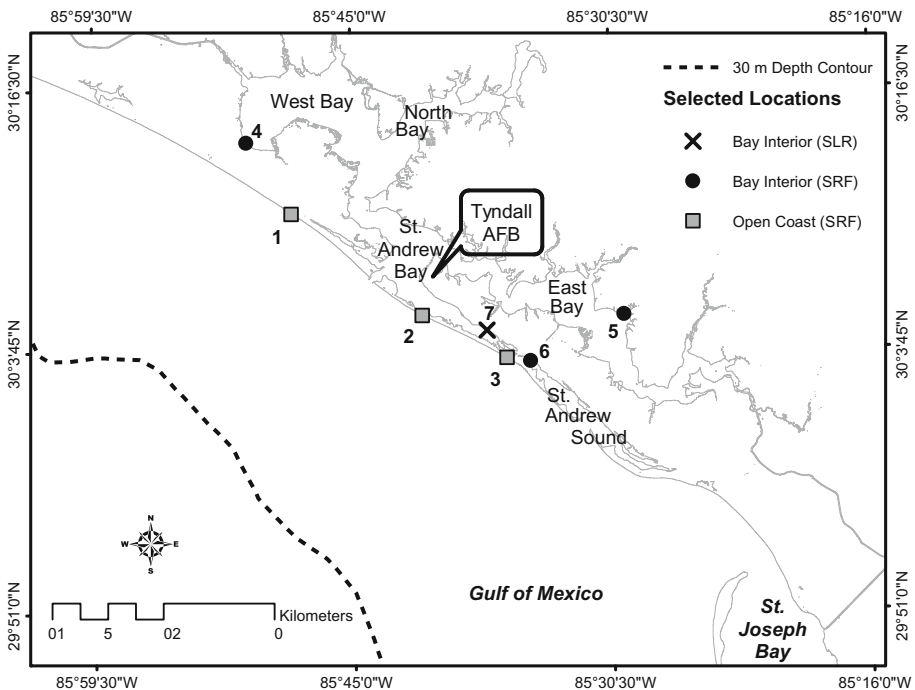


**Fig. 1** Panama City, FL location map

term climate trends, such as increases in sea surface temperatures (SST) or MSL, introduce nonstationarity into these probabilistic assessments. This can result in a change in surge exposure with time, and its quantification is important for effective long-term community planning. Long-term SLR is mainly driven by thermal expansion and ice sheet losses, primarily from Greenland and Antarctica (e.g., Rahmstorf 2007; Solomon 2007; Pfeffer et al. 2008; Yin et al. 2011). Future SLR projections, based on six global emission scenarios, are provided by the Intergovernmental Panel on Climate Change (Solomon 2007). These projected increases, which range from 0.18 to 0.59 m by the year 2100 for the lowest (B1) and highest (A1FI) respective scenarios, do not include contributions from ice sheet losses (hereafter “cryospheric,” Solomon 2007); currently, the greatest source of uncertainty in SLR projections (NOAA 2012). Estimates that incorporate cryospheric contributions range from 0.50 to 1.40 m (Rahmstorf 2007) and from 0.79 to 2.01 m (Pfeffer et al. 2008).

The National Oceanic and Atmospheric Administration (NOAA) presents four recommended SLR projections for the year 2100. The two lower end scenarios are based solely on either observations of historical data, or thermal contributions to SLR (NOAA 2012). Scenarios representing the intermediate-high and highest projections (1.2 and 2.0 m) consider both thermal expansion and cryospheric sources; the intermediate-high scenario represents an average of multiple semi-empirical-based global SLR projections (NOAA 2012). Pfeffer et al. (2008) provides the basis for the highest scenario projection.

Rising sea levels can affect surge generation by altering shallow water depths and distances (e.g., Smith et al. 2010), coastal evolution (e.g., Irish et al. 2010; Passeri et al. 2015), and land cover (e.g., Irish et al. 2013; Bilskie et al. 2014), any of which may increase the likelihood of future flooding. Dynamic SLR effects on hurricane surge are generally small at open coast locations, if significant changes in coastal topography do not occur; examples of this are provided in Mousavi et al. (2011) for Corpus Christi, TX, and Lin et al. (2012) for New York City, NY. Other coastal regions, such as open coast locations near New Orleans, experience considerable differences in surge heights that correspond to coastal wetland losses from encroaching SLR (e.g., Smith et al. 2010). These dynamic peak surge effects were caused by the flooded marshlands becoming a large, shallow extension of the Gulf of Mexico (Smith et al. 2010), effectively increasing the shallow water distance available for surge generation.

The capacity of SLR to dynamically alter surge generation by affecting coastal land cover changes was reported by Irish et al. (2013) for the area near Bay St. Louis, MS. Here, bottom friction changes due to SLR encroachment on protective coastal wetlands have caused significant surge momentum loss reductions. The dynamic SLR effects on surge generation near Bay St. Louis are on the order of 0.5–1.0 m, for surge heights greater than 6.0 m (Irish et al. 2013); these effects are comparable with those resulting from the shallow water distance increases observed in Smith et al. (2010). Bilskie et al. (2014) also examine dynamic SLR effects on surge generation, with respect to changes in land cover and land use (LCLU), for Mississippi Sound and Mobile Bay, AL. When changes in LCLU due to urbanization as well as SLR are considered, dynamic surge effects are confirmed for coastal wetland areas; however, surge effects for many other locations become more static and less dynamic (Bilskie et al. 2014).

Significant changes in SLR-induced surge response can also be expected within coastal bay interiors (e.g., Mousavi et al. 2011; Bilskie et al. 2014). Mousavi et al. (2011) investigated the surge response characteristics of Corpus Christi Bay, a shallow bay enclosed by low-elevation barrier islands. Locations inside Corpus Christi Bay, sufficiently spaced from the barrier islands, showed significant reductions in surge generation with respect to SLR increases. It is estimated that future barrier island degradation induced by SLR will contribute an additional 0.3 m to surge elevation in Corpus Christi Bay during moderate

surge events (Irish et al. 2010). Thus, it is likely that the bathymetric and geographic features of coastal bays, including inlet geometry and the characteristics of any existing barrier islands, will impact SLR-based surge response.

### 1.3 Surge response functions

SRFs are physics-based algebraic expressions of hurricane surge; once developed, these equations can replace the expensive computational models associated with traditional JPM applications. Irish and Resio (2013) define the JPM, in terms of return period, as a continuous probability density function (PDF) of storm parameters:

$$T_Z = \left\{ 1 - \int_{c_p} \int_{R_p} \int_{v_f} \int_{\theta} \int_{x_0} f(c_p, R_p, v_f, \theta, x_0) H(Z - [\phi(x, c_p, R_p, v_f, \theta, x_0, \text{MSL}) + \varepsilon_z]) dx_0 d\theta dv_f dR_p dc_p \right\}^{-1} \tag{1}$$

where  $Z$ , total maximum flood elevation;  $T_Z$ , total maximum flood elevation return period;  $x$ , location of interest;  $\phi$ , SRF model term;  $c_p$ , Hurricane central pressure;  $R_p$ , Hurricane radius of maximum winds;  $v_f$ , Hurricane forward velocity;  $\theta$ , Hurricane track angle;  $x_0$ , Hurricane landfall position; MSL, mean sea level;  $f$ , joint probability density function (see “Appendix”); () indicates the parameter is a function of the variable in parentheses.

The Heaviside function ( $H$ ) in Eq. 1 represents the nonexceedance limit, where  $H(x) = 1$  when  $x \geq 0$ , and  $H(x) = 0$  otherwise.

SRFs are developed using dimensionless surge scaling terms, which are derived from the shallow water momentum equations. Song et al. (2012) developed the following SRF model, which incorporates hurricane central pressure (hereafter intensity), storm size, and  $L_{30}$  influences into the dimensionless alongshore surge response, for open coast application:

$$\zeta' = \frac{\gamma_0 \zeta}{\Delta p} + m_2(x, x') \left( \frac{\Delta p}{\Delta p_{\max}} \right)^{\alpha(x, x')} \left( \frac{R_p/L_{30}(x_0)}{[R_p/L_{30}]_{\text{ref}}} \right)^{\beta(x, x')} \tag{2a}$$

$$x' = \frac{x - x_0}{R_p} - \lambda(x_0) + cH\left(\frac{x - x_0}{R_p} - \lambda(x_0) - 1\right)H\left(\frac{L_{30}}{L_{30-\text{ref}}} - 1\right)\left(\frac{R_p}{L_{30}}\right) - F\left(1 - \frac{R_p}{R_{\text{thres}}}\right)H\left(1 - \frac{R_p}{R_{\text{thres}}}\right) \tag{2b}$$

$$F\left(1 - \frac{R_p}{R_{\text{thres}}}\right) = \begin{cases} a_1\left(1 - \frac{R_p}{R_{\text{thres}}}\right) + b_1 & \text{for } -\lambda \leq x' \leq 0 \\ a_2\left(1 - \frac{R_p}{R_{\text{thres}}}\right) + b_2 & \text{for } 0 < x' \leq \lambda \\ 0 & \text{for } \lambda < |x'| \end{cases} \tag{2c}$$

$$[m_2(x, x'), \alpha(x, x'), \beta(x, x')] = \begin{cases} [m_{2L}(x), \alpha_L(x), \beta_L(x)] & \text{for } x' < 0 \\ [m_{2R}(x), \alpha_R(x), \beta_R(x)] & \text{for } x' \geq 0 \end{cases} \tag{2d}$$

where  $x'$ , dimensionless alongshore parameter;  $\zeta'$ , dimensionless surge parameter;  $\zeta$ , peak surge elevation;  $\lambda(x_0)$ , dimensionless ratio between distance from hurricane eye at landfall and location of alongshore maximum peak surge location and  $R_p$ ;  $c$ , dimensionless regional

scaling constant;  $L_{30}$ , cross-shore distance from shoreline to 30-m bathymetric contour, at  $x_0$ ;  $L_{30\text{-ref}}$ , threshold value of  $L_{30}$ ;  $R_{\text{thres}}$ , threshold value of  $R_p$ ;  $a_1, a_2, b_1, b_2 =$  dimensionless scaling coefficients;  $m_2, \alpha, \beta$ , dimensionless scaling coefficients;  $\Delta p$ , ambient pressure and hurricane central pressure difference;  $\Delta p_{\text{max}}$ , maximum theoretical hurricane intensity (Tonkin et al. 2000);  $[R_p/L_{30}]_{\text{ref}}$ , maximum value of  $R_p/L_{30}$ ;  $\gamma_0$ , reference specific weight of water;  $()$  indicates the parameter is a function of the variable in parentheses.

This model was developed using high-resolution hydrodynamic surge simulations for the entire Texas coast and represents a physically based scaling of surge response. A main advantage of this optimal sampling approach, with respect to other approaches, is that it provides a physics-based method for estimating surge across the continuum of storm parameter possibilities. As such, complex processes inherent in the surge response, for example, the influence of rapid spatial changes in winds for small storms, are well represented by the model. As summarized in Irish et al. (2009) and Song et al. (2012), the first term in Eq. 2a represents the first-order momentum balance, while the second term captures additional wind drag effects and the influence of relative storm size ( $R_p/L_{30}$ ) on surge generation. The first term in Eq. 2b captures first-order alongshore surge distribution as a function of storm size. The second term in Eq. 2b captures the influence of relative storm size ( $R_p/L_{30}$ ) on the degree of asymmetry in alongshore surge distributions west and east of a storm’s landfall position. The third term in Eq. 2b is an adjustment for small storms making landfall near the location of interest, where the presence of the hurricane eye-wall has a relatively large influence on local surge generation. The model in Eq. 2 has two physically based regional constants,  $R_{\text{thres}}$  and  $L_{30\text{-ref}}$ , and three location-specific fit coefficients,  $m_2, \alpha$ , and  $\beta$ . The constant  $R_{\text{thres}}$  physically represents the upper limit of storm size for small storms whose compact eye-wall impacts local surge, while the constant  $L_{30\text{-ref}}$  physically represents the continental shelf width beyond which the relative storm size ( $R_p/L_{30}$ ) has a measureable influence on surge response. The fit coefficient  $m_2$  represents the relative significance of the higher-order wind drag effects at the specified location. The fit coefficients  $\alpha$  and  $\beta$  are weighting parameters with values ranging between zero and one and indicate the relative influence of hurricane intensity and size on dimensionless surge. All three fit coefficients are specified by regression analyses using solely the surge data at the location of interest. Song et al. (2012) reported negligible bias and a maximum root-mean-square (RMS) error of 0.22 m, when applying this form of the SRF model to the Texas open coast, significantly lower than the ADCIRC RMS error of 0.37 m when best available historical storm wind and pressure fields and historical tidal conditions are used, as reported by Westerink et al. (2008).

### 1.4 Epistemic uncertainty

Epistemic uncertainty is inherent in JPM population inputs created using hydrodynamic models and OS techniques. This uncertainty can be quantified by the standard deviation between actual and estimated flood elevations (e.g., Resio et al. 2009, 2013, Irish and Resio 2013) and is assumed to be normally distributed:

$$\varepsilon_z^2 = \varepsilon_{\text{tide}}^2 + \varepsilon_{\text{waves}}^2 + \varepsilon_{\text{winds}}^2 + \varepsilon_{\text{model}}^2 + \varepsilon_{\text{residual}}^2 \tag{3}$$

where  $\varepsilon_z$ , epistemic uncertainty;  $\varepsilon_{\text{tide}}$ , tide model uncertainty;  $\varepsilon_{\text{model}}$ , hydrodynamic and wind model uncertainty;  $\varepsilon_{\text{waves}}$ , wave model uncertainty;  $\varepsilon_{\text{wind}}$ , wind model uncertainty;  $\varepsilon_{\text{residual}}$ , residual uncertainty.

In JPM-OS sampling methods using the SRF approach, the model term in Eq. 3 represents the sum of variances for both the hydrodynamic and SRF models. The residual term

accounts for additional random modeling errors. Uncertainty estimates within the Gulf of Mexico region, before SRF contributions are considered, range between 0.70 m (Resio et al. 2013) and 1.0 m (Irish and Resio 2013). These values specifically reflect not only the surge model error, e.g., 0.37 m reported for ADCIRC (Westerink et al. 2008), but also error introduced by assuming idealized wind and pressure field forcing and the omission of astronomical tides within the ADCIRC simulations.

## 2 Methods

### 2.1 ADCIRC simulations

Hurricane simulations in the Bay County, FL area were computed using the two-dimensional, depth-integrated shallow water hydrodynamic model ADCIRC (Westerink et al. 2008) coupled with the SWAN wave model (Booij et al. 1999) to account for wave setup. The model employed the numerical grid used to produce Federal Emergency Management Agency (FEMA) digital flood insurance rate maps for the Florida panhandle and Alabama coastal region (University of Central Florida 2011), with coastline and bay interior resolution between 20 m and 100 m. Model validation (FEMA et al. 2011 draft report) against available high-water mark and water-level gauge data for Hurricanes Ivan (2004) and Dennis (2005) yields a model RMS error of 0.44 m and demonstrates that this model setup performs well in the study area. A nested hurricane vortex, planetary boundary layer (PBL) model (Thompson and Cardone 1996), with enhanced resolution over the northern Gulf of Mexico, was used to develop the wind and barometric pressure field inputs. Values for storm position, size, and central pressure were specified in 1-h intervals, and pressure and wind velocity fields were calculated in 15-min increments.

Surge simulations for 38 unique hurricane parameter combinations were carried out and analyzed to develop the SRFs, as a subset taken from those used in the recent FEMA study (University of Central Florida 2011). Parameter combinations for the 38 simulations were chosen so that sufficient variability would be present in the simulated surge data. Based on the findings in Irish et al. (2009) and Song et al. (2012), we used the following criteria, in order, to select the 38 storms:

1. The storm set should span with reasonable spatial coverage at the initial  $x'$  dimensionless parameter space given by the first term in Eq. 2b in order to ensure a suitable range of landfall positions, and storm sizes are included in the storm set;
2. The storm set should include a range of central pressures in order to ensure the storm set represents surges of different magnitudes;
3. The storm set should include a range of storm approach angles in order to ensure that uncertainty in the surge response due to this parameter is captured; and
4. The storm set should include a range of storm forward speeds in order to ensure that uncertainty in the surge response due to this parameter is captured.

Using these criteria, 20 distinct landfall positions were chosen based on initial  $x'$  estimates between  $-6.7$  (west) and  $3.0$  (east); the remaining parameter ranges are summarized in Table 1.

A second subset of seven storms was selected to evaluate the relationship between total flood elevation and SLR. Changes in sea level were modeled by statically increasing the water surface elevation throughout the computational domain. To simplify the analysis, localized differences in water surface elevation, sediment transport induced coastline



**Table 1** Parameter values for SRF hurricane simulations

Parameter	Minimum	Maximum	Total number of unique values represented
$\Delta p$	41 mb	105 mb	22
$R_p$	15 km	99 km	12
$v_f$	2.6 m/s	9.7 m/s	5
$\theta$	−61°	+73°	11

changes, barrier island degradation, LCLU changes, and other topographic adjustments were not considered. Each storm was simulated at SLR conditions of 0.0, 1.2, and 2.0 m, relative to MSL c. 2005.

### 2.2 SRF development

SRFs were developed for 73 open coast locations and 259 locations along the bay shoreline, following Song et al. (2012). The spacing between locations selected for SRF model development ranged between 0.5 and 1.5 km in the alongshore direction. A single term exponential or power distribution was applied to the dimensionless surge data (Eq. 2), in order to develop the best-fit algebraic model for each location. Values of  $L_{30}$ , at corresponding landfall locations, were interpolated from measurements taken at alongshore intervals of 30 km.

### 2.3 Uncertainty quantification

Use of the SRF and SLR models introduces additional uncertainty, beyond that directly associated with the hydrodynamic modeling. Here, epistemic uncertainties introduced by the SRF and SLR models were quantified using RMS errors as estimates of standard deviation, where the computed errors were determined to be normally distributed with an  $R^2$  of 0.93 or better at all locations with negligible bias. Total epistemic uncertainties were estimated by incorporating these SRF and SLR uncertainty terms into Eq. 3. Because hurricane exposure and tidal conditions are similar between the Louisiana-Mississippi study area analyzed in Resio et al. (2013) and the Panama City area, and because ADCIRC model area is comparable between the two locations, we assume the smaller total uncertainty estimate of 0.70 m from tide, wave, wind, computational model, and residual sources (Resio et al. 2013).

$$\varepsilon_z^2 = \varepsilon_{\text{tide}}^2 + \varepsilon_{\text{waves}}^2 + \varepsilon_{\text{winds}}^2 + \varepsilon_{\text{model}}^2 + \varepsilon_{\text{SRF}}^2 + \varepsilon_{\text{SLR}}^2 + \varepsilon_{\text{residual}}^2 \tag{4}$$

where  $\varepsilon_{\text{SRF}}$ , SRF uncertainty;  $\varepsilon_{\text{SLR}}$ , SLR model uncertainty.

## 3 Results and discussion

### 3.1 SRF development at open coast locations

Because of the region’s bathymetry, which features gradual changes in  $L_{30}$ , there was no significant correlation between the residual dimensionless surge, as computed by omitting the third term in Eq. 2b, and the third term in Eq. 2b. Thus, coefficient  $c$  in Eq. 2b was set

to zero. This indicates that the correction term for asymmetry in alongshore surge distributions, caused by changes in  $L_{30}$  values (Song et al. 2012), is not required for this area. A value of 30 km for  $R_{\text{thres}}$  in Eq. 2 was selected because it optimized performance of the SRFs (minimized RMS error) at the majority of bay and ocean locations. All other SRF parameters were determined through regression analysis.

Simulated surge data available for this study encompassed an alongshore distance of 98 km and did not include the alongshore maximum peak surge for most of the simulated hurricanes; therefore, an alternative to the Song et al. (2012) method of approximating the ratio of distance from landfall to location of peak surge and storm size,  $\lambda$ , was required. Initial SRF estimates were obtained using the following initial estimates of the dimensionless SRF:

$$x' = \frac{x - x_0}{R_p} \quad (5a)$$

$$\zeta' = \frac{\gamma_0 \zeta}{\Delta p} \quad (5b)$$

Values of  $\lambda$  were calculated as the deviation of the initial SRF's maximum value location from the dimensionless coordinate origin. Using this method, expected values of  $\lambda$ , ranging from 0.7 to 1.3, are obtained.

SRFs are presented in Fig. 2, for selected open coast locations. The selected locations include the alongshore reference location for bay interior SRFs, as well as locations near Panama City Beach and Tyndall Air Force Base (AFB). Locations near Panama City Beach and the bay reference point were selected for their geographic importance and are representative of open coast SRF performance. The location near Tyndall AFB was selected to examine worst-case model performance. A summary of  $R^2$ , RMS error, percent RMS error (hereafter %RMS error, computed as 100 times RMS error divided by the expected ADCIRC surge value), and bias values at the selected open coast locations is provided in Table 2.

Computed  $R^2$  values are 0.73 or better at all ocean locations, with 84 % of locations exhibiting an  $R^2$  of 0.80 or higher. This indicates the SRFs reasonably capture the natural trends in storm surge with meteorological parameters, especially when considering the relative simplicity of the SRF form in the context of the complexity of storm surge generation. RMS errors were below 0.40 m at 93 %, and below 0.30 m at 23 %, of the 73 open coast locations. These errors are comparable in magnitude to published ADCIRC model error of 0.37 m (Westerink et al. 2008) and to our study's ADCIRC model error of 0.44 m [20 %], illustrating that these two sources of uncertainty ( $\epsilon_{\text{model}}$  and  $\epsilon_{\text{SRF}}$  in Eq. 4) are of similar magnitude. Respective mean, minimum, and maximum RMS errors were 0.35, 0.25, and 0.47 m. With respect to expected ADCIRC surge, at open coast locations 97 % of %RMS errors were less than 30 %, while 69 % were less than 25 %. The Panama City open coast mean, minimum, and maximum bias values were  $-0.01$ ,  $-0.10$ , and  $+0.03$  m. RMS errors for the 73 open coast locations are higher than those reported in Song et al. (2012). A source of large alongshore RMS errors in this study, relative to those presented in Song et al. (2012), is the approximation of  $\lambda$  values at each SRF location.

### 3.2 SRF development at bay interior locations

Since the initial  $x'$  given in Eq. 5a represents the offset between peak open coast surge and landfall position, an adjustment for  $x$  is required in order to apply Eq. 2b at bay interior

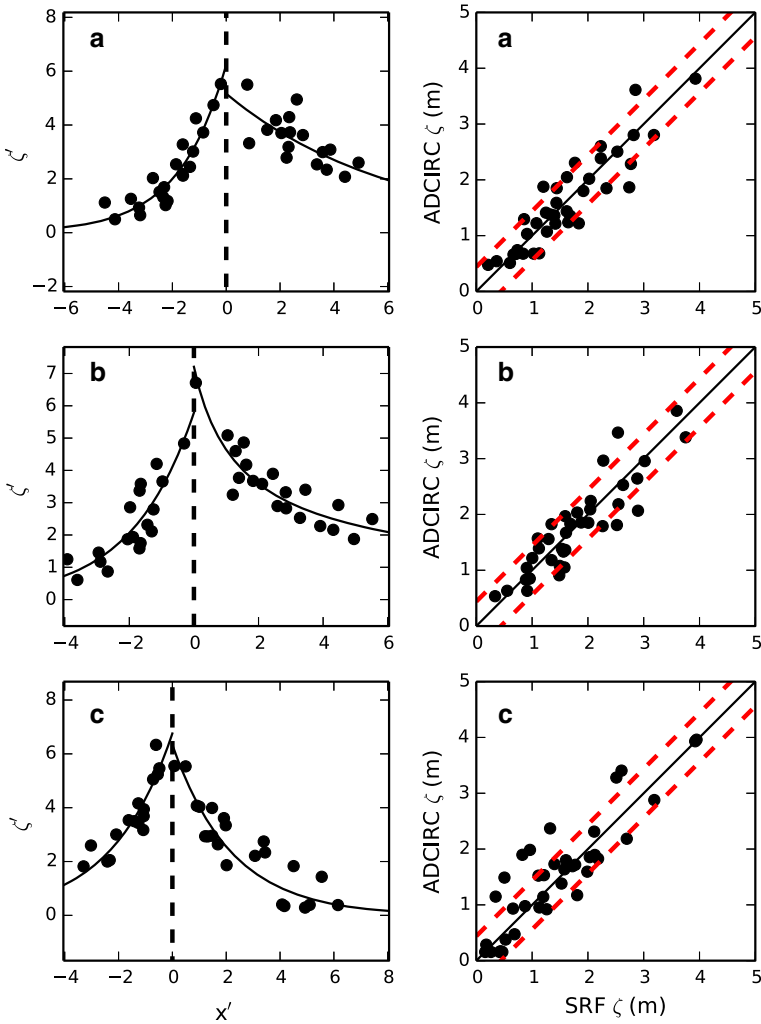


**Fig. 2** *Left* Surge response functions for selected open coast locations 1 (a Panama City Beach), 2 (b bay reference location), and 3 (c Tyndall Air Force Base). ADCIRC-simulated data are represented as *black circles*. *Solid lines* indicate best-fit regression models to ADCIRC data. *Dashed lines* show the dimensionless maximum peak alongshore surge location. *Right* ADCIRC-simulated versus SRF-predicted peak surge for selected open coast locations. ADCIRC-simulated data are represented as *black circles*. *Solid lines* indicate an exact match. *Dashed lines* show  $\pm 0.44$  m deviations (ADCIRC model error) about an exact match

locations. An alongshore reference value for  $x$  was selected by optimizing the performance (minimizing RMS error) of Eq. 2 for all 259 bay interior locations. The selected reference point corresponded to an alongshore distance of approximately half of the bay width (Fig. 1) and can be considered to represent the along-coast location that best represents the open coast surge contribution to bay surge. Values of  $\lambda$  in Eq. 2b were approximated for each bay interior station using the same methods described for open coast locations. The  $\lambda$  value at the reference location was used for the small storm adjustments in Eq. 2c. SRF performance was quantified by evaluating  $R^2$ , bias, and RMS error.

**Table 2** Performance statistics of SRF models at selected open coast (top) and bay interior (bottom) locations

Station	$R^2$	RMS error (m) [%RMS error (%)] (m)	Bias (m)
1	0.83	0.35 [22]	+0.02
2	0.80	0.37 [21]	+0.03
3	0.80	0.47 [30]	-0.10
4	0.76	0.38 [23]	+0.03
5	0.74	0.31 [23]	+0.01
6	0.67	0.61 [27]	+0.02

SRF models at bay interior locations, selected from the West Bay, East Bay, and St. Andrew Sound, are shown in Fig. 3. Locations inside the West Bay and East Bay were chosen to evaluate SRF performance at different bay interior regions, which are representative of bay interior SRF performance. The St. Andrew Sound location was selected to examine worst-case model performance. A summary of  $R^2$ , RMS error, and bias at the selected bay interior locations are summarized in Table 2.

Computed  $R^2$  values are 0.65 or better at all ocean locations, with 89 % of locations exhibiting an  $R^2$  of 0.70 or higher and 26 % exhibiting an  $R^2$  of 0.80 or higher. While these correlation statistics are not high as for ocean stations, we conclude that these algebraic SRFs provide a reasonable approximation of bay storm surge, whose response is highly variable owing to complex bay shorelines and bathymetry, for extreme value analysis so long as the error introduced by the SRFs is accounted for in such analyses. RMS errors were below 0.50 m at 96 %, below 0.40 m at 76 %, and below 0.30 m at 3 % of the 259 bay interior locations; these again are comparable with published ADCIRC model error of 0.37 m for storm surge (Westerink et al. 2008). With respect to expected ADCIRC surge, at open coast locations 87 % of %RMS errors were less than 30 %, while 69 % were less than 25 %. Mean, minimum, and maximum RMS errors were 0.39, 0.29, and 0.61 m, respectively. Bay interior mean, minimum, and maximum biases for all locations were -0.01, -0.12, and +0.05 m.

### 3.3 Surge adjustments for SLR

Figure 4 shows the total inundated areas for one ADCIRC-simulated hurricane at present day, 1.2, and 2.0 m of SLR, for the Panama City region. Under present day conditions, the barrier islands remain dry at most locations; this substantially limits floodwater access to bay interior locations. At 1.2 m SLR conditions, barrier island protection is substantially reduced, and floodwater access to bay interior locations within St. Andrew Bay and St. Andrew Sound is largely unhindered. Additional increases in SLR result in further barrier island inundation; however, these increases become less significant under SLR conditions of 2.0 m. The ADCIRC simulations conducted here to evaluate dynamic SLR impacts on surge generation did not account for potential morphological changes such as barrier island break-up or roll-over. Incorporation of these changes can potentially impact surge levels (e.g., Woodruff et al. 2013; Bilskie et al. 2014).

For all storms simulated, inundation of barrier islands under large SLR has a greater effect on nearby bay interior regions. Under present day conditions, hurricane surge in St. Andrew Bay is considerably less than surge magnitudes along the open coast. The difference in surge levels between bay location 7 and open coast location 3, under present day conditions, ranges from 0.25 to 0.98 m. With SLR, barrier island overtopping causes flood

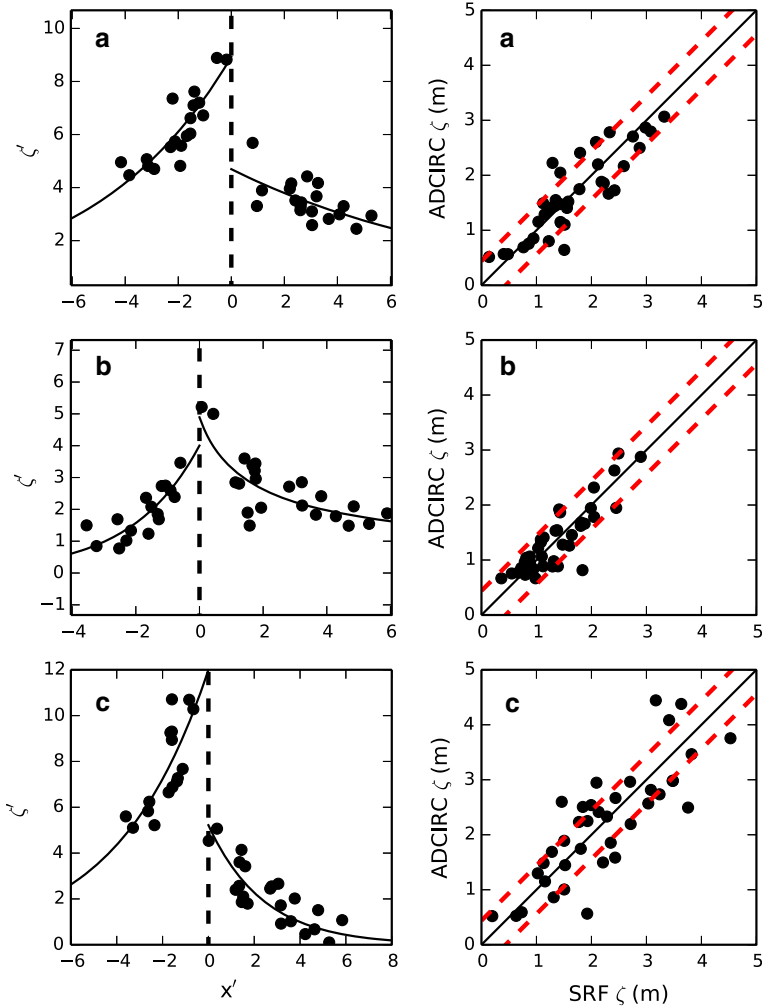


**Fig. 3** *Left* Surge response functions for selected bay interior locations 4 (a West Bay), 5 (b East Bay), and 6 (c St. Andrew Sound). ADCIRC-simulated data are represented as *black circles*. *Solid lines* indicate best-fit regression models to ADCIRC data. *Dashed lines* show the dimensionless maximum peak alongshore surge location. *Right* ADCIRC-simulated versus SRF-predicted peak surge for selected bay interior locations. ADCIRC-simulated data are represented as *black circles*. *Solid lines* indicate an exact match. *Dashed lines* show  $\pm 0.44$  m deviations (ADCIRC model error) about an exact match

levels in the easternmost sections of St. Andrew Bay to merge with the Gulf Coast flood levels. Surge differences between these locations (relative to open coast location 3) under 1.2 m and 2.0 m of projected SLR fall to respective ranges of  $-0.06$  to  $+0.42$  m, and  $-0.09$  to  $+0.19$  m. Rising sea levels cause surge magnitudes within east St. Andrew Bay to approach open coast values, as encroaching SLR reduces the separation between the bay interior and the Gulf Coast.

Significant reductions in surge generation occur with increasing SLR conditions in the western sections of St. Andrew Sound. In contrast to most other bay interior regions, St.

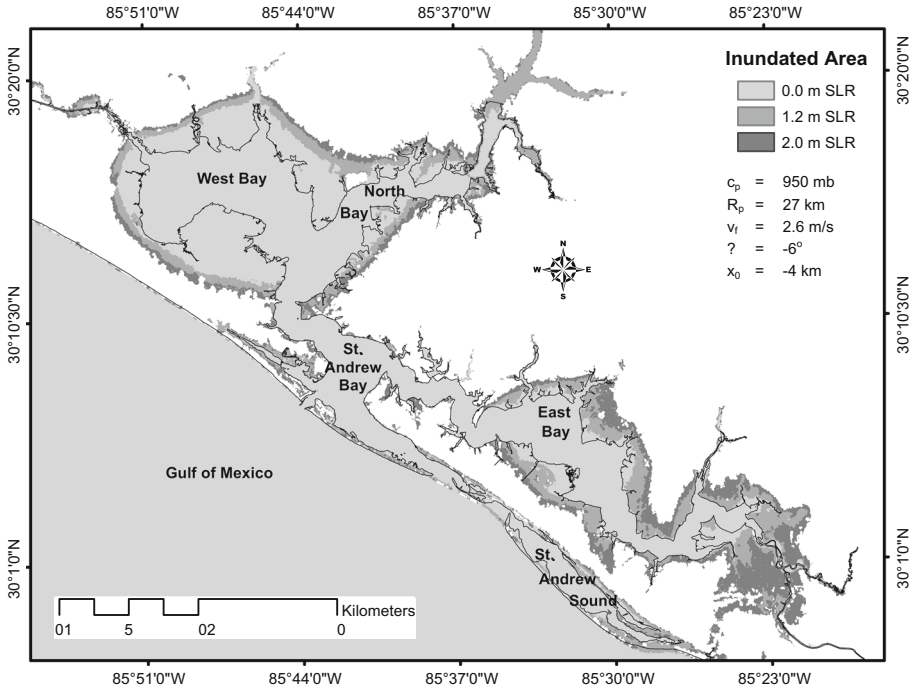


**Fig. 4** Total inundated areas for selected ADCIRC-simulated hurricane at present day, 1.2 and 2.0 m of SLR. An alongshore landfall position of  $-4$  km corresponds to Grayton Beach (latitude  $-86.18$ , longitude  $30.30$ )

Andrew Sound experiences higher surge generation at present day MSL, relative to open coast locations. With increasing SLR, surge magnitudes within the sound approach those at open coast locations. Compared with present day conditions, this results in an overall decrease in surge generation. St. Andrew Sound represents a small portion of Panama City’s total bay area; furthermore, this effect is confined to the western portion of the sound. Despite this localized decrease in surge, the data shown here provide evidence of a significant increase in the total flooding hazard, inclusive of SLR and surge changes.

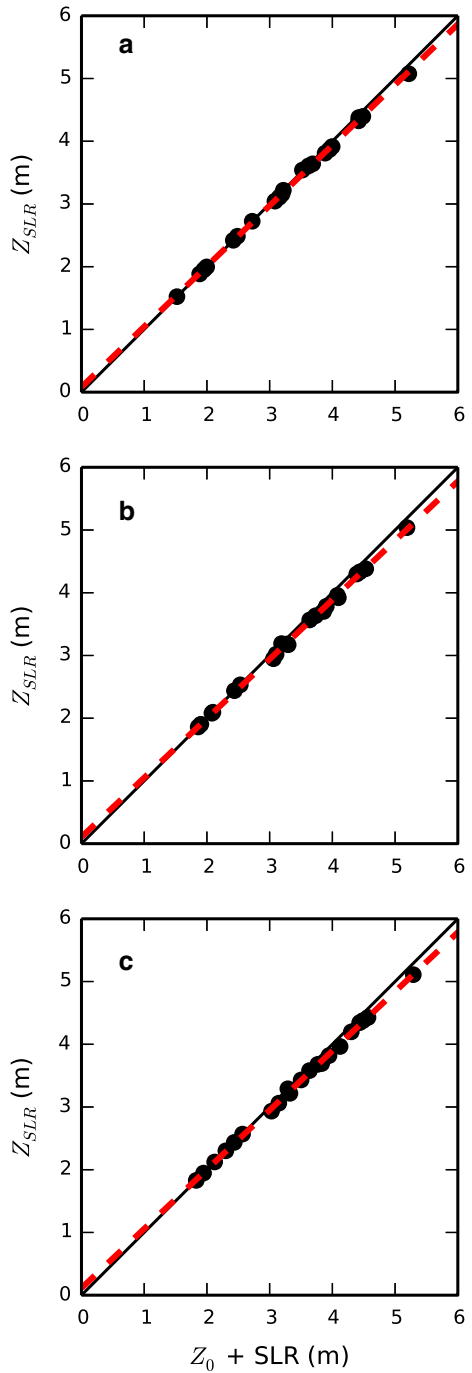
Surge trends with SLR were evaluated and quantified at each open coast and bay interior location by examining the simulated surge data. The summation of present day flood elevations ( $Z_0$ ) and SLR ( $Z_0 + \text{SLR}$ ) was compared with the ADCIRC-simulated total flood elevations under corresponding SLR conditions. The data exhibited the following trend:

$$Z_{\text{SLR}} = k(Z_0 + \text{SLR}) + l \tag{6}$$

where  $Z_{\text{SLR}}$ , total flood elevation at projected SLR, relative to present day MSL;  $Z_0$ , present day total flood elevation;  $k$ ,  $l$ , location-dependent fit coefficients; SLR, SLR, relative to present day conditions.

Performance of Eq. 6 was quantified by evaluating the  $R^2$ , bias, RMS error, and %RMS error. A value of  $k = 1$  suggests that the influence of SLR on surge generation is small, and that the total flood elevation can be approximated as the summation of SLR and present day flood elevation.

**Fig. 5** Total flood elevation trends at selected open coast locations 1 (**a** Panama City Beach), 2 (**b** bay reference location), and 3 (**c** Tyndall Air Force Base). ADCIRC-simulated data are represented as *black circles*. *Dashed lines* indicate best-fit regression models to ADCIRC data. *Solid lines* indicate an exact match



The summation of present day simulated flood elevation and SLR was compared with total simulated flood elevations under corresponding SLR conditions, at selected open

coast (Fig. 5) and bay interior (Fig. 6) locations. An additional location in the eastern section of St. Andrew Bay, where SLR effects on surge generation are significant, was also evaluated. The mean, minimum, and maximum RMS errors for all open coast locations were 0.03, 0.02, and 0.16 m, respectively, where 98 % of locations have a %RMS error of 1 % or less. Among the bay interior locations, the respective mean, minimum, and maximum RMS errors were 0.10, 0.02, and 0.36 m, where 95 % of locations have a %RMS error of 7 % or less. Bias was negligible ( $<0.005$  m) for all open coast and bay interior locations. The slope ( $k$ ) for the Panama City region, shown in Fig. 7, varies from 0.83 to 1.15.

The open coast trends shown in Fig. 5 display slope ( $k$ ) terms as low as 0.95 near the barrier islands, indicating that total flood elevations for many Panama City open coast locations cannot be approximated as static SLR increases. West Bay locations (Fig. 6a) show evidence of dynamic effects with similar magnitudes. Substantially high SLR effects

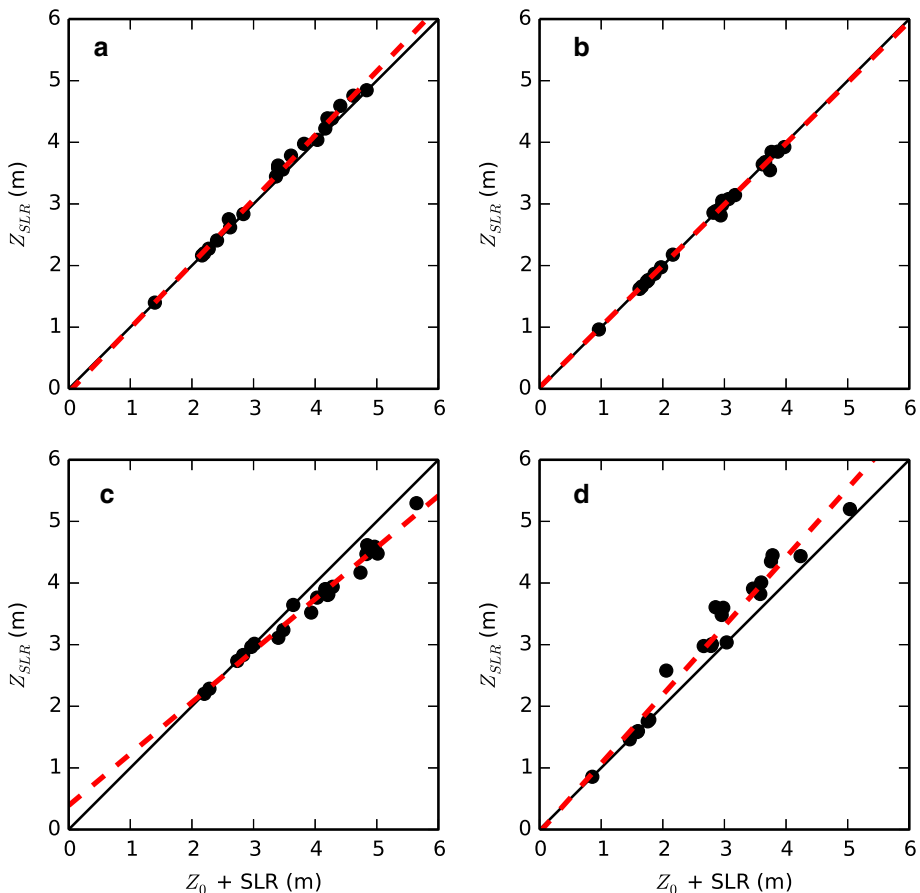


**Fig. 6** Total flood elevation trends at selected bay interior locations 4 (a West Bay), 5 (b East Bay), 6 (c St. Andrew Sound), and 7 (d St. Andrew Bay). ADCIRC-simulated data are represented as black circles. Dashed lines indicate best-fit regression models to ADCIRC data. Solid lines indicate an exact match



on surge are indicated by  $k$  values of 1.15 for the St. Andrew Bay location, and 0.85 for the St. Andrew Sound location. Figures 5 and 6 also provide evidence of highly correlated trends between SLR and total flood elevations, for both open coast and bay interior locations.

The spatial distribution of  $k$ , as shown in Fig. 7, is determined primarily by the geometry of coastline or bay interior features. Along the open coast, values of  $k$  decrease at locations close to the shoreline; these changes occur in a predominately alongshore direction. It can be observed, however, that the rate of decrease is not consistent for the entire area. Decreases in  $k$  occur more gradually for open coast locations in the west, while eastern locations show slightly accelerated  $k$  value decreases.

Within the bay interior, spatial distributions of  $k$  show trends that change with different bay geometries. In the West Bay, which has a comparatively large width relative to its length,  $k$  gradients are directed predominately to the northwest. St. Andrew Bay, which has outlets to the North Bay and East Bay, displays gradients in  $k$  that are directed toward these outlets. North Bay, East Bay, and St. Andrew Sound, which have much longer lengths relative to their widths, feature well-defined  $k$  gradients that are directed along their lengths.

SLR effects on surge generation within the bay interior undergo a transition from amplification in western areas to deamplification toward the east. Values of  $k$  at bay interior locations are above 1.00 for West Bay, St. Andrew Bay, and most of North Bay; this indicates surge amplification with increasing SLR. Transitions to surge deamplification, with  $k$  values below 1.00, occur in North Bay and East Bay locations. This effect is

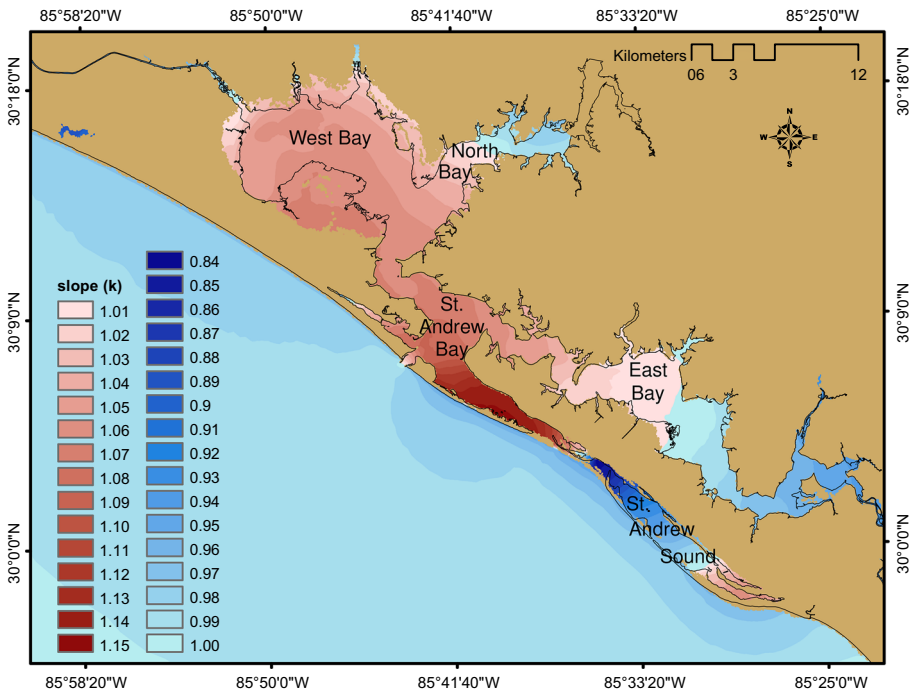


Fig. 7 Dynamic sea-level rise trends for the Panama City region ( $k$  coefficient from Eq. 6)

**Table 3** Total epistemic uncertainty, SRF model uncertainty, and SLR model uncertainty at selected open coast (top) and bay interior (bottom) locations

Loc.	$\varepsilon_{\text{new}}$ (m)	$\varepsilon_{\text{SRF}}$ (m)	$\varepsilon_{\text{SLR}}$ (m)	% Total increase
1	0.78	0.08	<0.01	10
2	0.79	0.09	<0.01	12
3	0.84	0.14	<0.01	17
4	0.80	0.10	<0.01	12
5	0.77	0.07	<0.01	9
6	0.93	0.22	0.01	25
7	0.90	0.16	0.03	22

Values are based on an initial uncertainty estimate of 0.70 m

most pronounced in East Bay, where  $k$  is as low as 0.94. The overall transition between amplification and deamplification corresponds with the shift from relatively steep elevation gradients in western Bay County areas to milder gradients in the east (Fig. 7). The existence of milder elevation gradients will likely result in surge deamplification, at the cost of greater overland inundation extent, as SLR increases.

### 3.4 SRF and SLR model contributions to epistemic uncertainty

Total epistemic uncertainty values, including SRF and SLR contributions, as well as the initial uncertainty value of 0.70 m, are provided in Table 3 for selected open coast locations and bay interior locations. Mean, minimum, and maximum SRF uncertainty contributions among all open coast locations were 0.08, 0.04, and 0.14 m, respectively. The mean, minimum, and maximum SRF uncertainty contributions among all bay interior locations were 0.10, 0.06, and 0.22 m. Mean SLR uncertainty contributions among all open coast and bay interior locations were negligible.

The initial uncertainty value of 0.70 m was selected to examine SRF and SLR error contributions to represent the worst case. Thus, the relative influence of uncertainty added by the SRF and SLR models will decrease when considering the larger base value of 1.0 m. In summary, we have demonstrated that the SRF and SLR models developed for Panama City, FL, marginally increase mean epistemic uncertainties by 0.08 m for open coast locations, and 0.10 m for bay interior locations.

## 4 Conclusions

By extending the SRF approach described in Song et al. (2012) to bay interior locations, an expression for estimating extreme surge values has been developed for Panama City, FL. These SRFs incorporate the primary statistical parameters associated with hurricane hazard assessments: central pressure, radius, and landfall location. An adjustment model incorporating dynamic SLR effects into total flood elevation estimates has also been proposed for open coast and bay interior locations. The Panama City SRFs showed RMS error values that were somewhat higher than those reported by Song et al. (2012); we hypothesize that the approximation for  $\lambda$  likely contributes to this additional error. Nonetheless, it has been demonstrated that the additional uncertainty from the SRF and SLR models presented in this study does not contribute significantly to the overall epistemic uncertainty in hazard analysis, and the approximate method used to determine  $\lambda$  makes the SRF approach more universally applicable when applied to datasets of limited spatial extent.

In this study, flood elevation adjustment accuracies were limited due to the absence of SLR-induced topographic changes (e.g., barrier island degradation, shoreline morphology.) in the ADCIRC hydrodynamic simulations. While such changes are not expected to be significant in the Panama City study area (Passeri et al. 2015), these coastal evolution impacts may have a significant impact on future surges in other locations. Land cover changes have been shown to alter surge generation near coastal wetlands (e.g., Smith et al. 2010; Irish et al. 2013); however, land cover effects on surge levels can range between +80 and −100 % over an entire region (Bilskie et al. 2014). Changes in land use due to urbanization can potentially increase surge generation by up to +70 % (Bilskie et al. 2014). Therefore, future research is recommended which incorporates SLR-induced topographic and land cover changes, as well as land-use changes from urbanization projections, into the SLR adjustments.

Dynamic SLR effects on surge generation are significant for the Panama City area and cause total flood elevations to be poorly characterized as static SLR increases. These dynamic effects are greatly influenced by characteristics such as topographic gradients, coastline geometry, and other regional geographic features and will vary significantly depending on coastal location (e.g., Hagen and Bacopoulos 2012; Bilskie et al. 2014). Therefore, it is necessary to study the physical surge dynamics using computational models, for each unique coastal region, to inform SRF and SLR development.

JPM applications coupled with the SRF model presented here can be used to provide useful hazard assessments on a regional scale. By extending model development to bays, the geographic restrictions limiting JPM-OS applications coupled with SRFs to open coast locations have been removed. The developed linear SLR adjustments represent a straightforward means for improving future coastal flood hazard assessments when significant coastal erosion is not expected or predictions of future erosion are not available. Furthermore, the high-resolution coastline and bay shoreline at which SRFs were developed can be used by coastal planners and developers to create flood inundation maps, damage assessments, and other applications useful for surge hazard mitigation.

**Acknowledgments** This material is based on the work supported by the National Sea Grant College Program of the U.S. Department of Commerce’s National Oceanic and Atmospheric Administration (Grant No. NA10OAR4170099. The views expressed here do not necessarily reflect the views of this organization. The STOKES ARCC (Advanced Research Computing Center) at the University of Central Florida provided computational resources for storm surge simulations (System. Administrators: P. Wiegand and G. Martin). The authors wish to thank Dr. James, M. Kaihatu, and Patrick W. McLaughlin, for their contributions to this work.

## Appendix

The joint probability density function,  $f$ , in Eq. 1 for the JPM-OS is defined as:

$$f(c_p, R_p, v_f, \theta, x_o) = A_1 A_2 A_3 A_4 A_5 \tag{7a}$$

$$A_1 = f(c_p|x_o) = \frac{1}{a_1(x_o)} \exp \left[ -\frac{\Delta p - a_o(x_o)}{a_1(x_o)} \right] \exp \left\{ -\exp \left[ -\frac{\Delta p - a_o(x_o)}{a_1(x_o)} \right] \right\} \tag{7b}$$

$$A_2 = f(R_p|c_p) = \frac{1}{\sigma(\Delta p)\sqrt{2\pi}} \exp \left\{ -\frac{[\mu(\Delta p) - R_p]^2}{2\sigma^2(\Delta p)} \right\} \tag{7c}$$

$$A_3 = f(v_f|\theta) = \frac{1}{\sigma(\theta)\sqrt{2\pi}} \exp\left\{-\frac{[\mu(\theta) - v_f]^2}{2\sigma^2(\theta)}\right\} \quad (7d)$$

$$A_4 = f(\theta|x_o) = \frac{1}{\sigma(x_o)\sqrt{2\pi}} \exp\left\{-\frac{[\mu(x_o) - \theta]^2}{2\sigma^2(x_o)}\right\} \quad (7e)$$

$$A_5 = \text{Rate of storm landfall occurrence per unit coastal length} \quad (1f)$$

where  $f$  = probability density functions;  $a_1$ ,  $a_2$  = Gumbel coefficients;  $\mu$  = mean of normal distribution;  $\sigma^2$  = variance of normal distribution; () indicates the parameter is a function of the variable in parentheses.

## References

- Bilskie MV, Hagen SC, Medeiros SC, Passeri DL (2014) Dynamics of sea level rise and coastal flooding on a changing landscape. *Geophys Res Lett* 41:927–934
- Booij N, Ris RC, Holthuijsen LH (1999) A third-generation wave model for coastal regions: 1. Model description and validation. *J Geophys Res* 104(C4):7649–7666
- Condon AJ, Sheng YP (2012) Optimal storm generation for evaluation of the storm surge inundation threat. *Ocean Eng* 43:13–22
- Fallah MH, Sharma JN, Yang CY (1976) Simulation model for storm surge probabilities. *Coast Eng Proc* 1(15):934–940
- Hagen SC, Bacopoulos P (2012) Coastal flooding in Florida's big bend region with application to sea level rise based on synthetic storm analysis. *Terr Atmos Ocean Sci* 23(5):481–500
- Irish JL, Resio DT (2013) Method for estimating future hurricane flood probabilities and associated uncertainty. *J Waterw Port Coast ASCE* 139(2):126–134
- Irish JL, Resio DT, Cialone MA (2009) A surge response function approach to coastal hazard assessment. Part 2: quantification of spatial attributes of response functions. *Nat Hazards* 51(1):183–205
- Irish JL, Frey AE, Rosati JD, Olivera F, Dunkin LM, Kaihatu JM, Ferreira CM, Edge BL (2010) Potential implications of global warming and barrier island degradation on future hurricane inundation, property damages, and population impacted. *Ocean Coast Manag* 53:645–657
- Irish JL, Sleath A, Cialone MA, Knutson TR, Jensen RE (2013) Simulations of Hurricane Katrina (2005) under sea level and climate conditions for 1900. *Clim Change* 122(4):635–649
- Lin N, Emanuel K, Oppenheimer M, Vanmarcke E (2012) Physically based assessment of hurricane surge threat under climate change. *Nat Clim Change* 2(6):462–467
- Liu D, Pang L, Fu G, Shi H, Fan W (2006) Joint probability analysis of hurricane Katrina 2005, vol 3. In: *Proceeding of international offshore and polar engineering conference, San Francisco, USA*, pp 74–80
- Mousavi ME, Irish JL, Frey AE, Olivera F, Edge BL (2011) Global warming and hurricanes: the potential impact of hurricane intensification and sea level rise on coastal flooding. *Clim Change* 104(3–4):575–597
- Niedoroda AW, Resio DT, Toro GR, Divoky D, Das HS, Reed CW (2010) Analysis of the coastal Mississippi storm surge hazard. *Ocean Eng* 37(1):82–90
- Parris A et al (2012) Global sea level rise scenarios for the United States National Climate Assessment. NOAA Technical Report OAR CPO-1. National Oceanic and Atmospheric Administration, Silver Spring
- Passeri DL, Hagen SC, Bilskie MV, Medeiros SC (2015) On the significance of incorporating shoreline changes for evaluating coastal hydrodynamics under sea level rise scenarios. *Nat Hazards* 75(2):1599–1617. doi:10.1007/s11069-014-1386-y
- Pfeffer WT, Harper JT, O'Neil S (2008) Kinematic constraints on glacier contributions to 21st-century sea-level rise. *Science* 321(5894):1340–1343
- Rahmstorf S (2007) A semi-empirical approach to projecting future sea-level rise. *Science* 315(5810):368–370
- Resio DT, Boc SJ, Borgman L, Cardone V, Cox A, Dally WR et al (2007) White paper on estimating hurricane inundation probabilities. US Army Corps of Engineers Engineer Research and Development Center, Vicksburg

- Resio DT, Irish J, Cialone M (2009) A surge response function approach to coastal hazard assessment—part 1: basic concepts. *Nat Hazards* 51(1):163–182
- Resio DT, Irish JL, Westerink JJ, Powell NJ (2013) The effect of uncertainty on estimates of hurricane surge hazards. *Nat Hazards* 66(3):1443–1459
- Smith JM, Cialone MA, Wamsley TV, McAlpin TO (2010) Potential impact of sea level rise on coastal surges in southeast Louisiana. *Ocean Eng* 37(1):37–47
- Solomon S (ed) (2007) *Climate change 2007—the physical science basis: working group I contribution to the fourth assessment report of the IPCC, vol 4*. Cambridge University Press
- Song YK, Irish JL, Udoh IE (2012) Regional attributes of hurricane surge response functions for hazard assessment. *Nat Hazards* 64(2):1475–1490
- Thompson EF, Cardone VJ (1996) Practical modeling of hurricane surface wind fields. *J Waterw Port Coast ASCE* 122(4):195–205
- Tonkin H, Holland GJ, Holbrook N, Henderson-Sellers A (2000) An evaluation of the thermodynamic estimates of climatological maximum potential tropical cyclone intensity. *Mon Weather Rev* 135:746–764
- Toro GR, Niedoroda AW, Reed CW, Divoky D (2010) Quadrature-based approach for the efficient evaluation of surge hazard. *Ocean Eng* 37(1):114–124
- University of Central Florida (2011) *Flood insurance study: Florida Panhandle and Alabama, model validation*. Report. Federal Emergency Management Agency, Philadelphia, PA
- Westerink JJ, Luettich RA, Feyen JC, Atkinson JH, Dawson C, Roberts HJ, Powell MD, Dunion JP, Kubatko EJ, Pourtaheri H (2008) A basin-to channel-scale unstructured grid hurricane storm surge model applied to southern Louisiana. *Mon Weather Rev* 136(3):833–864
- Woodruff JD, Irish JL, Camargo SJ (2013) Coastal flooding by tropical cyclones and sea-level rise. *Nature* 504(7478):44–52
- Yang CY, Parisi AM, Gaither WS (1970) Statistical prediction of hurricane storm surge. *Coast Eng Proc* 1(12):2011–2030
- Yin J, Overpeck JT, Griffies SM, Hu A, Russell JL, Stouffer RJ (2011) Different magnitudes of projected subsurface ocean warming around Greenland and Antarctica. *Nat Geosci* 4(8):524–528